Biomedicine & Pharmacotherapy 153 (2022) 113398

Contents lists available at ScienceDirect

Biomedicine & Pharmacotherapy

journal homepage: www.elsevier.com/locate/biopha

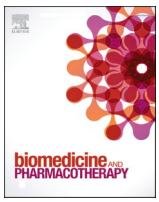

The BR2 peptide associated with 2-aminoethyl dihydrogen phosphate is a formulation with antiproliferative potential for a triple-negative breast cancer model

Laertty Garcia de Sousa Cabral [a,b,*], Henrique Hesse [a,b], Katielle Albuquerque Freire [c], Cyntia Silva de Oliveira [c], Cibele Nicolaski Pedron [d], Monique Gonçalves Alves [a,b], Julio Pacheco Carlstron [a,b], Jean-Luc Poyet [e,f], Vani X. Oliveira Jr [c,d], Durvanei A. Maria [a,b,*]

[a] Faculty of Medicine, University of Sao Paulo, FMUSP, Sao Paulo, Brazil
[b] Laboratory of Development and Innovation, Butantan Institute, Sao Paulo, Brazil
[c] Federal University of Sao Paulo, UNIFESP, Sao Paulo, Brazil
[d] Federal University of ABC, Center for Natural and Human Sciences, Santo Andre, Brazil
[e] Université Paris Diderot, Sorbonne Paris Cité, 75013 Paris, France
[f] INSERM UMRS976, Institut De Recherche Saint-Louis, Hôpital Saint-Louis, Paris, France

ARTICLE INFO

Keywords:
Nano molecules
Triple-negative breast cancer
Peptide
Monophosphoester
Synergism

ABSTRACT

Triple-negative breast cancer is the most aggressive subtype of breast cancer, with worse clinical evolution and tumor-free survival, leading to the need to develop new effective therapies for its control. The present study evaluated the action of tumor-penetrating peptide BR2 associated with 2-aminoethyl dihydrogen phosphate (2-AEH_2P) on triple-negative breast tumor cells. Cell viability was evaluated by the MTT colorimetric method, mitochondrial electrical potential, and proteins involved in cell proliferation and death control were evaluated by flow cytometry and structural and morphological analysis by confocal microscopy. The results obtained showed that the peptide BR2 and the association 2-AEH_2P + BR2 promoted significant cytotoxicity in tumor lines, compared to 2-AEH_2P alone. In addition, the association 2-AEH_2P + BR2 promoted tumor cells arrest in the G0/G1 phases. Interestingly, both treatments modulated the expression of markers CD44, CD34, CD24, cyclin D1, and Bcl-2, increased p21, Bax, and released cytochrome c. The association proved to be more effective, providing modulation of proteins involved in cell death and senescence, more pronounced cytotoxicity for tumor cells compared to normal cells, and the reduction of markers related to aggressiveness profile, progression, and tumor metastasis.

1. Introduction

Cancer is the main public health problem in the world and is already among the four main causes of premature death in most countries [1]. Breast cancer is the most recurrent neoplasm among women worldwide [1,2]. The triple-negative subtype (TNBC) is an aggressive, highly invasive cancer that accounts for about 15% of all breast cancers [3]. Compared with other subtypes, the survival time of patients with TNBC is shorter and the mortality rate is 40% in the first 5 years after diagnosis, with a recurrence rate of 25% after surgery [4–6].

Nano molecules have shown promise for specific target therapies, offering solutions for the treatment of numerous diseases. These molecules' greater efficacy and safety are due to their unique characteristics, allowing the incorporation of several support components, facilitating their solubilization, protection against degradation, and sustained release of numerous drugs, thus improving the balance between their effectiveness and systemic toxicity [7,8].

The synthetic peptide BR2 is a non-specific tumor-penetrating derivative of the peptide buforin II (21 amino acid residue α-helical with complete sequence identity to the N-terminal region of histone H2A), showing high tumor cells specificity, with membrane translocation efficiency four to six times higher in tumor cells compared to normal cells [9]. BR2 cellular uptakes rely on a unique mechanism that does not involve membrane lysis but rather an endocytic transport, binding to the

* Corresponding authors at: Faculty of Medicine, University of Sao Paulo, FMUSP, Sao Paulo, Brazil.
E-mail addresses: laertty.c@usp.br (L.G. de Sousa Cabral), durvanei.maria@butantan.gov.br (D.A. Maria).

https://doi.org/10.1016/j.biopha.2022.113398
Received 13 April 2022; Received in revised form 4 July 2022; Accepted 8 July 2022
Available online 15 July 2022

neuropilin-1 receptor and activating the transport pathway [10–13].

2-aminoethyl dihydrogen phosphate (2-AEH$_2$P) is a lipid monophosphoester involved in membrane turnover, being a precursor in the synthesis of several membrane phospholipids. Its antiproliferative and pro-apoptotic effect has been evidenced in several tumor cell lines, such as triple-negative human breast cancer cells (MDA MB-231) [14], human breast adenocarcinoma (MCF-7) [15], chronic myeloid leukemia (K562 e K562 Lucena MDR+) [16], hepatocellular carcinoma (Hepa1c1c7) [17] and melanoma (B16-F10) [18,19]. Furthermore, 2-AEH$_2$P induces apoptosis of immature cells in the spleen, and the liver in an in vivo model of RAR+ acute myeloid leukemia [18].

Considering the limiting factors of the therapies offered for the treatment of triple-negative breast cancer, the development of new drugs that present less systemic and tissue toxicity with a better response to treatment is essential. The objective of this work was to evaluate the effect of the BR2 peptide associated with 2-AEH$_2$P on human (MDA MB-231) and murine (4T1) triple breast cancer cells.

2. Materials and methods

2.1. Solid-phase peptide synthesis (SPPS), purification, and analysis

The peptides were synthesized on a peptide synthesizer (PS3-Sync Technologies) using solid-phase peptide syntheses, fluoromethyloxycarbonyl (Fmoc) strategy, and Rink Amide resin (substitution degree of 0.52 mmol g−1).17 After synthetic steps, the dry peptidyl resins were deprotected by TFA/anisole/water solution, as detailed by Torres et al. [20]. The crude peptides were precipitated with anhydrous diethyl ether, extracted with 60% acetonitrile in water, and lyophilized. Then, all peptides were purified by semipreparative reverse-phase high--performance liquid chromatography (RP-HPLC) on a Delta Prep 600 (Waters Associates), and the selected fractions containing the purified peptides were pooled and lyophilized. The purified peptides were characterized by liquid-chromatography electrospray-ionization mass spectrometry (LC/ESI-MS) using a Model 6130 Infinity mass spectrometer coupled to a Model 1260 HPLC system (Agilent), according to Torres et al. [20]. After the purification process, had been obtained an aqueous solution of the purified peptide. To obtain a solid material, the peptide solution was firstly cooled down to − 20 °C and then connected to the freeze-dryer Christ Alpha 2–4 LD plus (Serie 17937), at − 90 °C and a pressure low of 0.01 mbar for 2–3 days, until the complete water sublimation.

HELIQUEST calculates the physicochemical properties and amino acid composition of an α-helix to identify protein segments that have similar characteristics. The analysis module displays for each generated segment a table with net charge z (at pH = 7.4), average hydrophobicity <H> and hydrophobic moment < μH> calculated with a standard hydrophobicity scale, as well as statistics on its composition. Net charge (z) is the net positive charge experienced by an electron in a multi-electron atom. Mean hydrophobicity <H> is a property exhibited by solids to repel water. Hydrophobic moment < μH> is the vector sum of the hydrophobicity values of each residue present in the polypeptide sequence.

2.2. Cell culture

The cell lines cultures were as follows, triple-negative MDA MB-231 human breast cancer (ATCC® CRM-HTB-26), murine breast cancer 4T1 (ATCC® CRL-2539), normal human endothelium HUVEC (ATCC® CRL-1730), and normal human fibroblast FN1. The cell lines were grown in RPMI-1640 medium (LGC Biotecnologia, Cotia, SP, Brazil), except the MDA MB-231 line that was grown in Leibovitz medium (LGC Biotecnologia, Cotia, SP, Brazil). The media was supplemented with 2 mM L-glutamine (Cultilab, Campinas, SP, Brazil), 10 mM HEPES (Cultilab, Campinas, SP, Brazil), 24 mM sodium bicarbonate, 0.01% antibiotics, and 10% fetal bovine serum (FBS) (Cultilab, Campinas, SP, Brazil). The cells were cultivated in a 5% CO_2 atmosphere at 37 °C. A viability assessment was performed using the Trypan Blue exclusion test, proceeding when cell viability was over 94%.

2.3. MTT cytotoxicity assay

Tumor and normal cells were incubated in 96-well plates at 1×10^5 cells/mL for 24 h and 48 h and treated with the BR2 peptide, 2-AEH$_2$P, and the combination of 2-AEH$_2$P + BR2 in different concentrations. The treatment with the association was based on the fixed concentration of 2-AEH$_2$P and varied concentrations of the BR2 peptide. The IC50 values obtained for each cell were considered, being fixed to half of the IC50 value of 2-AEH$_2$P per well and the BR2 peptide in different concentrations. After 24 h and 48 h of treatment, the supernatant was aspirated and 100 μL of 5 mg/mL MTT (Calbiochem – Darmstadt, Germany) was added, the cells were incubated for 3 h in an atmosphere containing 5% CO_2 at 37 °C. Subsequently, the content was removed and 100 μL of methanol was added to dissolve the formazan crystals. The absorbance at 540 nm was then assessed using a microplate reader.

The IC50 values are obtained from the GraphPad Prism 5 program. After establishing the values of the “X” and “Y” axes, the data is normalized to a percentage (100%), the concentration values are converted into log values, then a linear regression, to open the "Dose-Response - Inhibition" equations tab and choose "log (inhibitor) vs. response, at the bottom of the dialog, select the option for "Interpolate unknowns from standard curve", ends and the IC50 values are obtained.

2.4. Analysis of cell cycle phases and fragmented DNA by flow cytometry

The cells were subjected to treatments for a period of 24 h. The treated and control cells were trypsinized and centrifuged at 1200 rpm for 5 min. Then, the pellet was resuspended in a solution of 70% alcohol and RNAse alcohol and stored at − 20ºC for 24 h. The samples were centrifuged at 1500 rpm for 10 min and resuspended in 200 μL of FACS buffer, 20 μL of Triton X-100 (Sigma-Aldrich), and 50 μg/mL of propidium iodide (Sigma- Aldrich), maintained for 30 min at room temperature while protected from light. The samples were then transferred to cytometry tubes and taken for analysis on a FACScanto (BD) flow cytometer at FLH-1 fluorescence intensity by the number of events (10.000 events) and the histograms acquired and analyzed by the software CellQuest - BD.

2.5. Evaluation of cell markers expression by flow cytometry

Control or treated MDA MB-231 (10^5 cells/mL) was incubated for 1 h at 4 ºC, with 1 μg of specific antibody conjugated to phycoerythrin. Several markers involved in cell death, regulators of cell cycle progression, adhesion, and angiogenesis were used, such as BAX, BCL-2, Cyclin D1, Cytochrome C, P21, CD44, CD34, CD24, and PCNA, conjugated in phycoerythrin-PE. After the cells were centrifuged at 1500 rpm and washed with cold PBS, the supernatant was discarded and the pellet was resuspended in 200 μL of FACS buffer containing 0.1% paraformaldehyde. The reading and analysis of the expression of receptors on the surface of tumor cells were performed in a flow cytometer FACScanto (BD) at fluorescence intensity FL1-H by the number of events (10.000 events) and the DotPlots acquired and analyzed by the program Cell-Quest- BD.

2.6. Analysis of mitochondrial electrical potential by flow cytometry

Control or treated tumor cell were centrifuged at 1500 rpm for 10 min, the supernatant was discarded and 5 μL of Rhodamine-123 (5 mg/mL diluted in ethanol) was added (Molecular Probes, USA). Then, the samples were incubated in 5% CO_2 at 37ºC for 30 min. Afterward, the tubes were centrifuged, the supernatant was discarded, and the pellet was resuspended in 100 μL of FACS Flow buffer. The reading and analysis of Rhodamine-123 staining on cells were performed in a

FACScanto flow cytometer (BD) at FL1-H fluorescence intensity per number of events (10.000 events) and the histograms were acquired and analyzed by the Cell-Quest - BD software.

2.7. Morphological evaluation by laser confocal microscopy

Tumor and normal cells were grown in 24-well plates containing round coverslips with respectively RPMI and Leibovitz medium supplemented with 10% FBS and incubated with 5% CO_2 at 37ºC for 24 h. The samples from the control and treated groups were subjected to the culture media removal process and washed with RPMI medium. 200 nML^{-1} of MitoRed (Sigma-Aldrich, USA) was then added and the cells were incubated for 1 h in the dark at 37° C. Following incubation, the cells were washed with PBS, incubated with MitoRed, and fixed with 4% paraformaldehyde for 30 min. The cells were then washed with PBS and incubated. 100 μL of phalloidin (Sigma-Aldrich, USA) for 1 h in the dark at room temperature. The excess phalloidin was removed and the cells were washed with a culture medium. The coverslips were placed on slides for observation in the Confocal Laser fluorescence microscope (Fluoview ™ 300) and the images were documented and analyzed.

2.8. SynergyFinder 2.0 analysis of multiple drug combinations

To determine the potential synergy of the drug, a matrix study was performed with the BR2 peptide and the 2-AEH_2P. The combination matrix was tested on two cell lines: MDA MB-231 and 4T1. SynergyFinder 2.0 software quantified the degree of synergy as the excess over the multiplicative effect of single drugs as if they acted independently (Bliss), the following higher-order formulations were used to quantify drug combination (S) synergy for the multiple drug combination effect measured between 2 drugs:

$$S_{BLISS} = E_{A,B} - (E_A + E_B)$$

$$SynergyScore = \frac{-10g(p)}{\log(0.05)} \times \frac{t}{|t|}$$

2.9. Statistical analysis

All values obtained from the different cell lines were expressed as mean ± standard deviation. After obtaining the individual values of each cell line, treated and controlled, the results were tabulated and analyzed using the software Graphpad, Version 5.0, and Version 7.0. Data analysis was performed by comparing two or more groups with nonparametric distribution using analysis of variance (ANOVA), followed by the TUKEY-KRAMER multiple comparison tests, considering $p \leq 0.05$ as the critical level for significance.

3. Results

3.1. Synthesis and purification of BR2 peptide

The crude peptide was purified by semi-preparative RP-HPLC and analyzed by mass spectrometry (Fig. 1 A-B). The purified peptide had a purity > 97% (Fig. 1 C). The physical-chemical properties data were calculated using the Helquist Freeware software [21]. It was observed that the peptide has the characteristic of being amphipathic because it has a hydrophobicity <H> of 0.48 and a hydrophobic moment <μH> of 0.4 after the sum of the charge of all the amino acids of the peptide. Characteristic that corroborates the presence of the α-helix present in the BR2 peptide. The observed net charge of + 6 evidences that the BR2

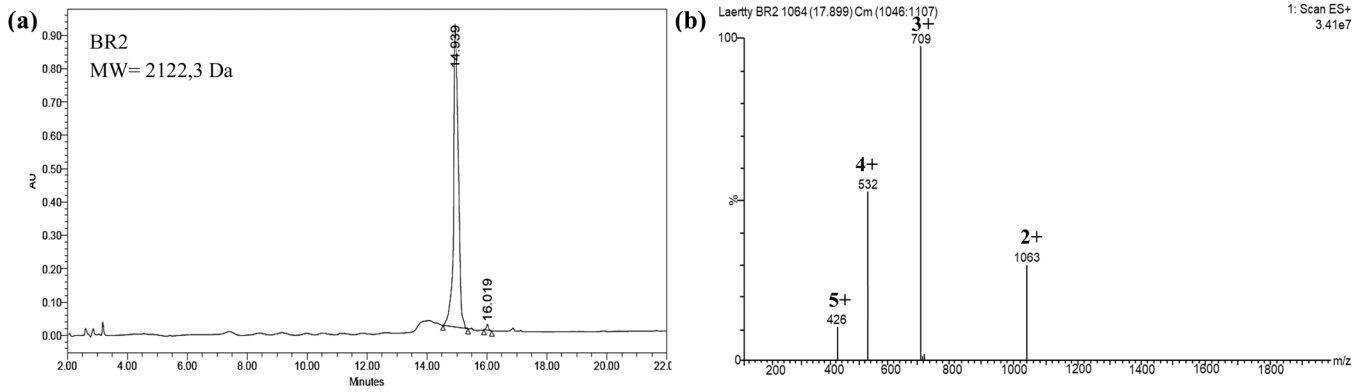

Peak Name	RT	Area	%Area	Height
1	9.323			
2	9.566			
3	10.284			
BR2	14.939	10022361	99.14%	9066640
	16.019	86580	0.86%	18526

(c)

Peptide	Sequence	Molecular weight (Da)		H	μH	z
		Calculated	Observed			
BR2	CRAGLQFPVGRLLRRLLR	2122,2	2126	0,48	0,4	+6

H (hydrophobicity), μH (hydrophobic moment), z (netload) according to Heliquest helical wheel projection.

Fig. 1. (a) Chromatogram; (b) Mass scan of BR2 in 17.899 min; *m/z*; (c) Degree of purity of the peptide; (d) physicochemical of the peptide obtained from the Heliquest Freeware program.

peptide is a cationic peptide, capable of interacting with electronegative regions of the tumor cell (Fig. 1 D).

3.2. Determination of cytotoxic activity

We next assayed the cytotoxicity effect of BR2 on the tumor breast cancer cells MDA MB-231 and 4T1 upon peptide, both 4T1 and MDA MB-231 cells showed loss of adhesion and changes in their morphology, such as cytoplasmic retraction, increased cytoplasmic volume, and cell fragmentation for all groups tested (Fig. 2 A). Dose-response analyses indicate that the IC50 values for 2-AEH$_2$P-mediated cell death of the4T1 tumor cells were 17.4 mM and 2.6 mM for 24 h and 48 h, respectively. The BR2 peptide and the association 2-AEH$_2$P + BR2 inhibited cell viability in all tested concentrations, resulting in an IC50 for BR2 for the periods of 24 h and 48 h of 28 μM and 18 μM, respectively. Interestingly, the association 2-AEH$_2$P + BR2 lowered the IC50 concentrations to 17.5 μM and 10 μM (Fig. 2 B-D). Treatment of MDA MB-231 tumor cells with increasing doses of 2-AEH$_2$P revealed IC50 values of 12 mM and 6.5 mM for 24 h and 48 h, respectively, while IC50 values for the BR2 peptide were 14 μM and 9.5 μM for 24 and 48 h. As witnessed for 4T1 cells, the 2-AEH$_2$P + BR2 association lowered the IC50 to 5.4 μM and 3.3 μM for 24 and 48 h. (Fig. 2 B-D).

Importantly, similar treatments of normal cells HUVEC and FN1 showed low toxicity, although there were slight changes in their morphology (Supplementary Figure 1 A). 2-AEH$_2$P did not induce significant cytotoxicity in HUVEC cells, with a calculated IC50 of 32 mM and 27 mM following 24 h and 48 h treatment. BR2 peptide promoted significant cytotoxicity at the highest concentrations tested, with IC50 of 39 μM and 42 μM for treatments of 24 h and 48 h, respectively, whereas the association 2-AEH$_2$P + BR2 exhibited an IC50 of 33.6 μM for a 24 h treatment and 33.3 μM for an 8 h treatment (Supplementary Figure 1 B). In normal FN1 cells, 2-AEH$_2$P did not induce significant cytotoxicity, with an IC50 of 56 mM and 41 mM for 24 h and 48 h treatments, respectively. The peptide BR2 showed moderate activities against FN1 cells, with IC50 values of 35 μM and 36 μM for 24 h and 48 h treatment. Finally, the IC50 values of the 2-AEH$_2$P + BR2 association were 29.5 μM and 27 μM for 24 h and 48 h of treatment (Supplementary Figure 1 B).

3.3. Cell cycle phases distribution analysis, fragmented DNA, and proliferation markers

Treatment of the 4T1 tumor cell line with 2-AEH$_2$P at 17 mM promoted a reduction in the G0/G1 phase and an increase in the S phase, with percentage values of 37.7 ± 3.2% and 37.3 ± 2.7% respectively, and an increase in fragmented DNA of 27.3 ± 2.6%. Treatment with the BR2 peptide at 28 μM caused a reduction in the G0/G1 phase (21.2 ± 2.1%), an increase in the S phase (65.4 ± 1.9%), and fragmented DNA (39.1 ± 0.9%). The association 2-AEH$_2$P + BR2 reduced the G2/M phase (18.6 ± 1.9%) and increased the population of cells in the S phase (36.7 ± 2.2%) and fragmented DNA (11.7 ± 3.1%) at the highest tested concentration (Fig. 3 A). The treatment of tumor cells MDA MB-231 with 12 mM of 2-AEH$_2$P promoted an increase in the G0/G1 phase (75.1 ± 1.4%) and fragmented DNA (20.9 ± 1.7%), reduction in the S phase (16.6 ± 2.7%). Treatment with the BR2 peptide did not result in a significant difference in the distribution of the cell cycle whereas DNA fragmentation increased considerably (29.7 ± 2.5%). Treatment with the association 2-AEH$_2$P + BR2 resulted in cell cycle phases alterations similar to that obtained with 2-AEH$_2$P, with a significant increase in the G0/G1 phase (72.4 ± 1.4%) and fragmented DNA (36.6 ± 3.9%) and reduction of cells in the S phase (22.8 ± 0.5%) at the highest tested concentration (Fig. 3 B).

A significant increase in p21 protein expression was observed after treatment of the MDA MB-231 cells with the BR2 peptide (67.1 ± 2.3%) and with the association 2-AEH$_2$P + BR2 (68.2 ± 3.5%) (Fig. 3 C). In contrast, the expression of cyclin D1 protein decreased following all treatments: with a reduction of 45.7 ± 0.3% upon 2-AEH$_2$P exposure, 41.1 ± 0.2% with the BR2 peptide) and 41.9 ± 0.7% with the association 2-AEH$_2$P + BR2 (Fig. 3 D). PCNA expression reduced significantly following treatments with the BR2 peptide (30.2 ± 1.0%) and 2-AEH$_2$P + BR2 association (38.1 ± 1.2%) (Fig. 3 E).

In HUVEC endothelial cells, treatment with 2-AEH$_2$P at 17 mM promoted an increase in the G0/G1 phase (69.9 ± 3.1%) without changes in the other cell cycle phases. The treatment with BR2 peptide at 20 μM resulted in a reduction in the S phase (19.1 ± 1.1%) and cell arrest in the G2/M phase (14.4 ± 0.9%). The association 2-AEH$_2$P + BR2 promoted an increase of cells in the G0/G1 phase (68.8 ± 1.2%) and a reduction of cells in the S phase (16.6 ± 0.5%) at the concentration of 20 μM. The treatments did not promote a considerable increase in fragmented DNA in the HUVEC endothelial cell (Supplementary figure 2 A). In normal human fibroblasts FN1 cells, treatment at the highest concentration of 2-AEH$_2$P reduced the fraction of cells in the G0/G1 phase (35.8 ± 2.1%), increased cells in the S phase (38.5 ± 1.8%) and DNA fragmentation (16.3 ± 1.9%). Treatment with the BR2 peptide did not cause any significant changes in the tested concentrations but increased the percentage of fragmented DNA (14.8 ± 0.8%). However, the association 2-AEH$_2$P + BR2 promoted an increase of cells in the G0/G1 phase in all tested concentrations, with values of 36.8 ± 2.1%, 53.2 ± 1.1%, and 51.5 ± 0.6% for the concentrations of 8 μM, 17 μM, and 35 μM of BR2 peptide and 28 mM of 2-AEH$_2$P, respectively, whereas, at the highest concentration, the fraction of fragmented DNA was 19.4 ± 2.4% (Supplementary figure 2 B).

3.4. Analysis of the electrical potential of the mitochondrial membrane (ΔΨm)

The analysis of the mitochondrial electrical potential by flow cytometry showed that there was a reduction in the mitochondrial electrical potential of the 4T1 tumor cells upon exposure to the BR2 peptide with a percentage value of 9.0 ± 1.21%, whereas 2-AEH$_2$P promoted a reduction of 11.5 ± 2.8% and the association 2-AEH$_2$P + BR2 promoted a reduction of 14.7 ± 1.25% (Fig. 4 A). MDA MB-231 tumor cells treated with BR2 peptide and 2-AEH$_2$P exhibited a reduction in mitochondrial electrical potential of 28.3 ± 3.8and 18.9 ± 1.9%, respectively, and the association 2 -AEH$_2$P + BR2 resulted in a reduction in mitochondrial electrical potential of 57.8 ± 2.9%. Of note, the control group had 9.3 ± 0.9% of non-viable mitochondria (Fig. 4 A).

The mitochondrial electrical potential of the tumor cells was evaluated from the fluorescence intensity of the photomicrographs captured in a confocal microscope. There was a reduction in ΔΨm in 4T1 tumor cells, with values of 35 ± 3.7% (BR2), 50.7 ± 4.1% (2-AEH$_2$P) and 89.6 ± 3.5% (2-AEH$_2$P + BR2) (Fig. 4B). These treatments promoted similar changes in MDA MB-231 tumor cells to those observed in 4T1 tumor cells, with a reduction in the mitochondrial electrical potential for the BR2 peptide of 71.2 ± 2.1%, when treated with 2-AEH$_2$P and association 2-AEH$_2$P + BR2, the reduction in mitochondrial electrical potential values was 82.6 ± 1.1% and 87.6 ± 1.8% respectively (Fig. 4 B).

Treatments of the normal HUVEC and FN1 cells at the IC50 concentrations to that of MDA MB-231 tumor cells did not result in a significant reduction in ΔΨm (Supplementary Figure 3 A-B). HUVEC cells treated with IC50 concentrations corresponding to that of 4T1 tumor cells exhibited a reduction of ΔΨm of 37.2 ± 3.4% for the BR2 peptide, 9.3 ± 0.9% for 2-AEH$_2$P, and 41.4 ± 2.5% for the 2-AEH$_2$P + BR2 association (Supplementary Figure 3 A). There was a reduction of ΔΨM for FN1 cells when treated with IC50 values of 4T1 tumor cells, with percentage values of 36.6 ± 1.3% for treatment with BR2 peptide, 15.8 ± 2.5% for 2-AEH$_2$P, and 42.4 ± 1.2% for the association 2-AEH$_2$P + BR2 (Supplementary Figure 3 B).

Corroborating the reduction of ΔΨM and already indicating the possible mechanism of action of the molecules and the association, flow cytometry analysis showed that there was a significant increase in the expression of Bax protein when treated with the BR2 peptide (67.1 ± 2.7%) and with the association 2-AEH$_2$P + BR2 (66.4 ± 1.9%), with

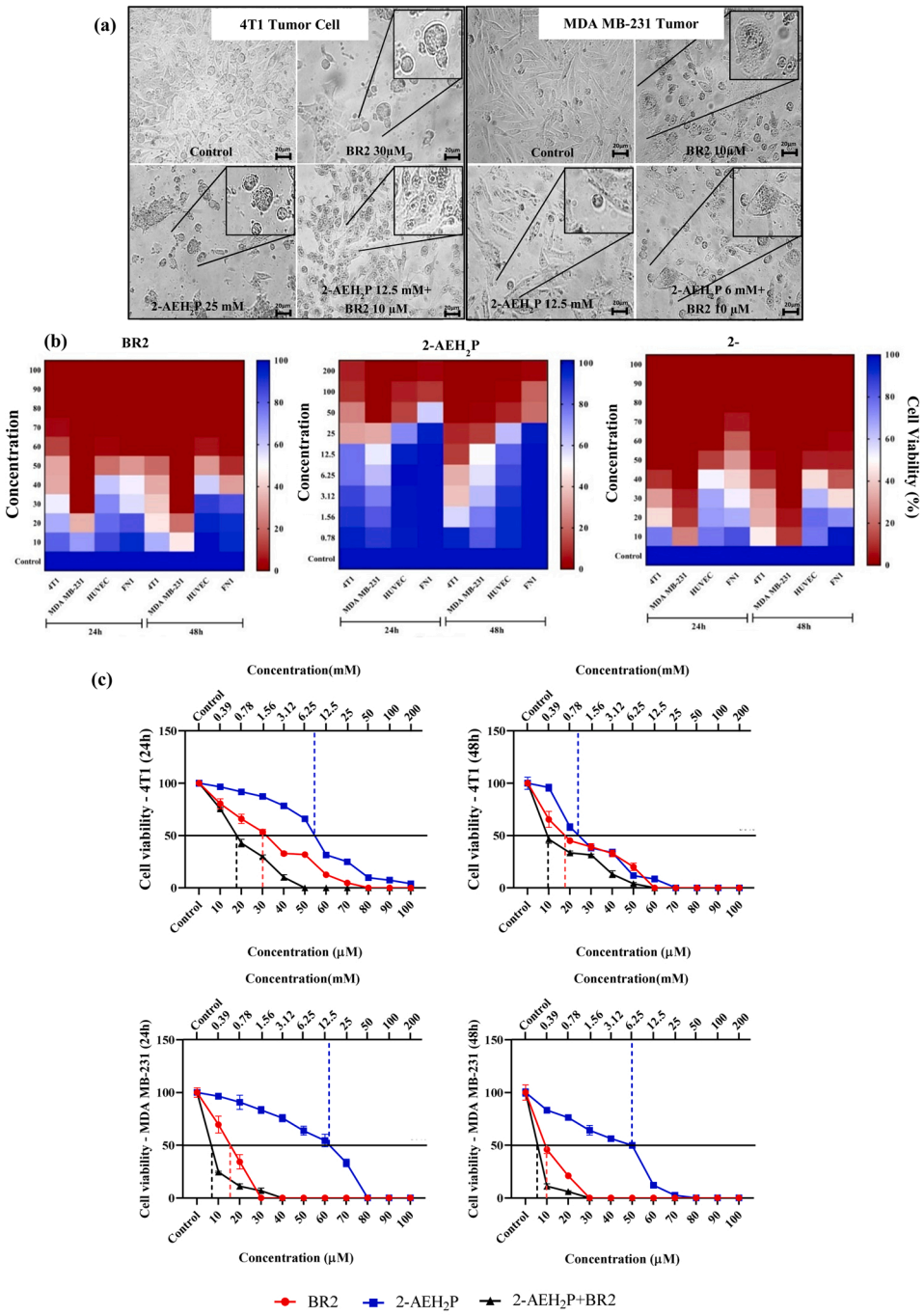

(d)

Cells	Treatment	Time	IC50
MDA MB-231 (Breast cancer human)	BR2	24h	14μM
	2-AEH$_2$P		12mM
	2-AEH$_2$P+BR2		5.4μM
	BR2	48h	9.5μM
	2-AEH$_2$P		6.5m
	2-AEH$_2$P+BR2		3.3μM
4T1 (Breast cancer murine)	BR2	24h	28μM
	2-AEH$_2$P		17.4 mM
	2-AEH$_2$P+BR2		17.5μM
	BR2	48h	18μM
	2-AEH$_2$P		2.6 mM
	2-AEH$_2$P+BR2		10 μM

Fig. 2. Determination of cytotoxicity in triple-negative human MDA MB-231 and murine 4T1 breast cancer tumor cells by the MTT colorimetric method. Cells were treated with different concentrations of BR2 peptide, monophosphester 2-AEH$_2$P, and the association 2-AEH$_2$P + BR2, for a period of 24 h and 48 h. (a) Photomicrographs of the morphological analysis of MDA MB-231 and 4T1 tumor cells treated in a 24 h period; (b) Line graph shows the correlation of the cytotoxic effect expressed as mean±SD of three independent experiments for tumor cells 4T1 and MDA MB-231 in the period of 24 h and 48 h; (c) The heatmap shows the correlation of the cytotoxic effect expressed as mean±SD of three independent experiments; (d) Table with IC50 values for murine MDA MB-231 and 4T1 triple-negative human breast cancer tumor cells.

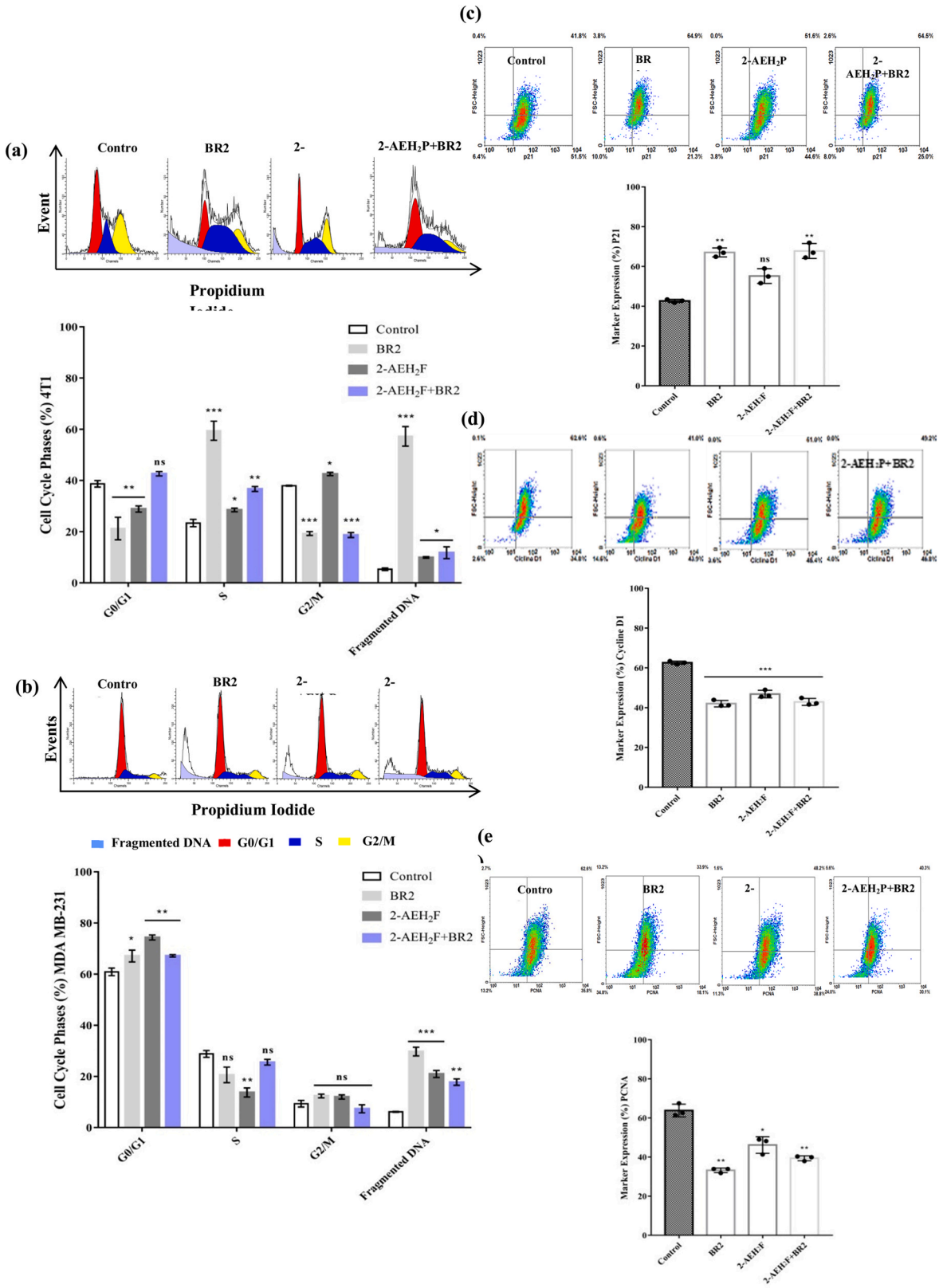

Fig. 3. Analysis of cell cycle phases in MDA MB-231 and murine 4T1 triple-negative human breast cancer tumor cells. The cells were treated with the peptide BR2, the monophosphoester 2-AEH$_2$P, and the association 2-AEH$_2$P + BR2, at IC50, for a period of 24 h and 48 h. (a) Distribution profile of 4T1 tumor cells in cell cycle phases; (b) Distribution profile of MDA MB-231 tumor cells in cell cycle phases; (c) Expression of P21 in MDA MB-231 tumor cell; (d) Expression of Cyclin D1 in MDA MB-231 tumor cell; (e) Expression of PCNA in MDA MB-231 tumor cell. Bar graph expressed as mean±SD of three independent experiments. Representative histograms of the distribution of cells in the phases of the cell cycle. Representative Density Plots show the distribution of cell numbers with fluorescence intensity. Statistical differences were obtained by ANOVA and Tukey-Kramer multiple comparison test. *$p < 0.05$, * *$p < 0.01$ and * **$p < 0.001$.

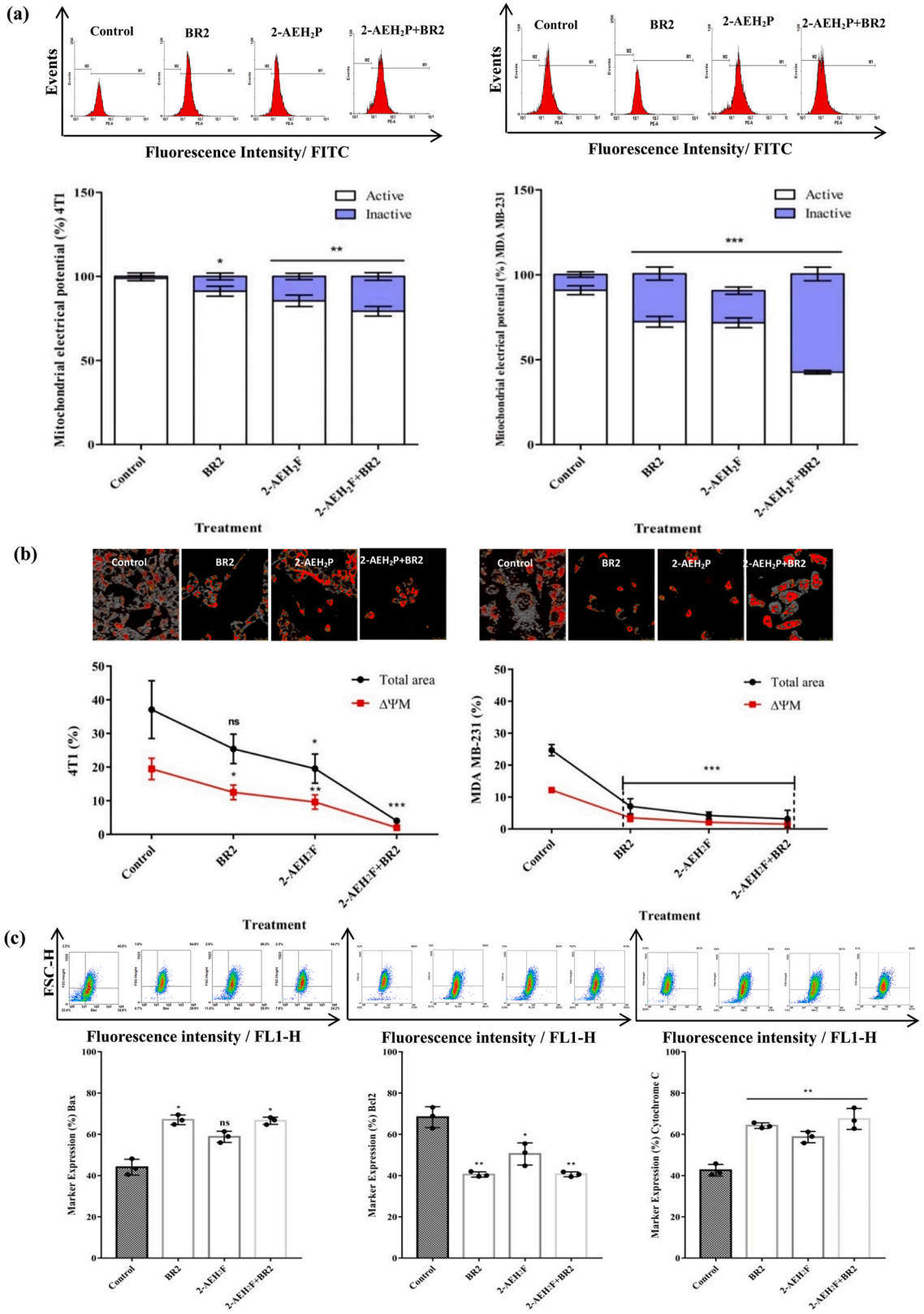

Fig. 4. Analysis of mitochondrial electrical potential (ΔΨm) in MDA MB-231 and murine 4T1 triple-negative breast cancer tumor cells. The cells were treated with the peptide BR2, the monophosphoester 2-AEH$_2$P, and the association 2-AEH$_2$P + BR2 at IC50 values for a period of 24 h. (a) ΔΨm of 4T1 and MDA MB-231 tumor cells; (b) ΔΨm of 4T1 and MDA MB-231 tumor cells and total area, analyzed by ImageJ; (c) Expression of Bax, Bcl2, and Cytochrome C release in MDA MB-231 tumor cell. Bar and line graph showing ΔΨm expressed as mean±SD of three independent experiments. Representative histograms of the distribution of cells in the phases of the cell cycle. Representative Density Plots show the distribution of cell numbers with fluorescence intensity. Statistical differences were obtained by ANOVA and Tukey-Kramer multiple comparison tests. *$p < 0.05$, * *$p < 0.01$ and * **$p < 0.001$.

no significant changes for treatment with 2-AEH$_2$P (Fig. 4 C). The expression of the anti-apoptotic protein Bcl-2 decreased significantly after treatment with 2-AEH$_2$P (50.4 ± 0.8%), BR2 peptide (40.8 ± 0.8%) and 2-AEH$_2$P + BR2 association (40.6 ± 0.5%) (Fig. 4 C). All treatments demonstrated induced apoptosis in this tumor lineage, mediating the release of cytochrome c to the cytoplasm, confirming the formation of mitochondrial membrane pores and consequent reduction of ΔΨM (Fig. 4 C).

3.5. Morphological evaluation by laser confocal microscopy

Confocal laser scanning microscopy examination of untreated cells revealed an intense marking of mitochondria with a granular appearance (red fluorescence), evenly distributed in the cytoplasm, and the cytoskeletal filaments well distributed, maintaining the original conformation of the cells (green fluorescence) (Fig. 5). Interestingly, treatments with either BR2, 2-AEH$_2$P, or the association 2-AEH$_2$P + BR2 promoted important morphological changes in the structural arrangement of the cytoskeleton of breast tumor cells 4T1 and MDA MB-231, indicating apoptosis, such as reducing mitochondrial electrical potential and redistributing mitochondria to the perinuclear region, and depolarization and reorganization of the cytoskeleton in the pericellular region.

Upon treatments, it was possible to observe in the tumor cells that cytoplasmic contraction resulted from depolarization and reorganization of the cytoskeleton filaments to the pericellular region. The active mitochondria were moved to the perinuclear region. With the association, extravasation of the cytoplasm into the extracellular environment was observed (Fig. 5).

In human endothelial cells, HUVEC, and human fibroblast FN1 the treatments with the values of IC50 of that of the tumor cell MDA MB-231 did not promote significant morphological changes, except for the 2-AEH$_2$P + BR2 association, that provided depolarization of the cytoskeleton in the FN1 cells (Supplementary Figure 4). When treated with the IC50 concentrations of 4T1 tumor cells, it was possible to observe important morphological changes. Indeed, HUVEC endothelial cells treated with the BR2 peptide the presence of more than one nucleus, characteristic of aberrant/catastrophic mitosis, in addition to the increased intracellular volume. The 2-AEH$_2$P treatment and the 2-AEH$_2$P + BR2 association presented depolarization of the cytoskeleton, promoting reorganization to the pericellular region and migration of the mitochondria to the perinuclear region (Supplementary figure 4). A similar cellular reorganization was observed in normal human fibroblast FN1 when treated with concentrations corresponding to the IC50 values of the 4T1 tumor cell (Supplementary Figure 4).

3.6. Analysis of progression and metastasis markers

Flow cytometric analysis of the markers involved in tumor progression, invasiveness and metastasis showed that there was a reduction in the expression of the CD44 marker after treatment with 2-AEH$_2$P (46.5 ± 0.7%), with the BR2 peptide (41 ± 2, 1%) and association 2-AEH$_2$P + BR2 (45.2 ± 2.4%) (Fig. 6 A). CD24 expression decreased significantly with all treatments, with a decrease of 41.3 ± 1.6%, when cells were treated with 2-AEH$_2$P, 38.4 ± 2.4%with the BR2 peptide treatment, and 32 ± 2.1% with the association 2-AEH$_2$P + BR2 (Fig. 6 B). When analyzing the expression of the CD34 marker, the only treatment that promoted a significant variation was with peptide BR2, promoting a reduction in the expression of the marker (Fig. 6 C).

3.7. Analysis of the synergistic effect of the BR2 peptide and 2-AEH$_2$P treatments

The antagonistic effect is observed in the colored space between white and green (≤0), the additive effect and synergism are observed in the colored space between white and red (> 0 and <10 additive; > 10 synergistic). The combinational activity of the BR2 peptide and 2-AEH$_2$P was investigated in the tumor cells of MDA MB-231 and 4T1 using SynergyFinder 2.0 with the Bliss analysis model. The most significant synergy was observed for tumor cells MDA MB-231 when treated with the association 2-AEH$_2$P + BR2, presenting a synergistic effect with a synergy score of 10.17 (Fig. 7 A). For 4T1 cells, the synergy score obtained was 5.97 (Bliss calculated), showing the additive effect of the molecules (Fig. 7 B).

4. Discussions

In this study, we analyzed the ability of the tumor penetrating peptide BR2 to potentiate the antitumor effects of 2-aminoethyl dihydrogen phosphate (2-AEH$_2$P) in human and murine triple-negative breast cancer tumor cells. Our results demonstrate a synergistic effect of the 2-AEH$_2$P + BR2 combination compared to the compounds used separately, resulting in a dramatic reduction of their IC50 when associated. There was modulation of proteins involved in cell death and progression, as well as depolarization and degradation of important intracellular structures such as the cytoskeleton and distribution of mitochondria, evidencing the ability of treatments to possibly modulate senescence pathways and selectively regulate cell death for this type of neoplasia.

Cell-penetrating cationic peptides have antiproliferative properties with varied molecular targets, from the nucleus to mitochondria, modifying several intracellular structures and thus triggering regulated cell death with high selectivity for tumor cells [21–23]. Studies have shown that the BR2 peptide has antitumor potential, inducing cytotoxicity in several tumor strains, such as HepG2 (hepatocarcinoma); HeLa (human cervical cancer); MCF-7 (human breast adenocarcinoma); HCT116 (human colon cancer); B16-F10 (murine melanoma) [24–26]. One of the main hypothesis for the selective cytotoxicity of cationic peptides in tumor cells is that the membranes of tumor cells have greater electronegativity due to the high expression of anionic components, such as heparan sulfate, phosphatidylserine, and sialic acid [27]. The peptide used in this study showed greater selectivity for tumor cells due to its net charge of + 6, thus increasing its antitumor potential.

2-Aminoethyl dihydrogen phosphate has been widely studied by our group and has broad antitumor potential and low systemic toxicity, inducing cytotoxicity in several tumor cell lines, such as EAT (Ehrlich's ascitic tumor) and H292 cells (human lung carcinoma) [28]; B16F10 cells (murine melanoma) [19]; MCF-7 cells (human breast adenocarcinoma) [15]; MB-231 MDA cells (human triple-negative breast cancer) [14]; Skmel-28 cells, Mewo (human melanoma) and Hepa1c1c7 cells (hepatocarcinoma) [17]; K562 and K562-Lucena (chronic myelogenous leukaemia-MDR +) [16].

In theory, the combination of drugs with different ways of action or different pharmacokinetic properties provides a better therapeutic response when using lower doses of each component than would be necessary for every single administration, with fewer serious adverse events [29,30]. The effect of combining the BR2 peptide and the 2-AEH$_2$P at lower concentrations was analyzed, showing greater toxicity for tumor cells, the data corroborate a possible additive effect for the tumor cell 4T1 and synergistic for cell tumor MDA MB-231, thus having its effects enhanced. Several studies have shown that tumor penetrating peptides potentiate the action of other molecules, in immunotherapy facilitating the permeabilization of these cells to the tumor microenvironment and, directing drugs in target-specific therapies [31,32].

Metastasis is a complex process that involves invasion and homing and proliferation at the sites of metastasis [33]. It was observed by Sheridan et. al (2006) that the CD44$^+$/CD24$^-$ phenotype is associated with an enhanced invasive capacity and elevated expression of genes involved in invasion in TNBC cells [34]. CD44 and CD24 have been shown to positively or negatively regulate breast cancer cell invasion and metastasis [35,36]. Yang et al. showed that blocking CD44 expression prevents the formation of local and metastatic tumor nodules in the

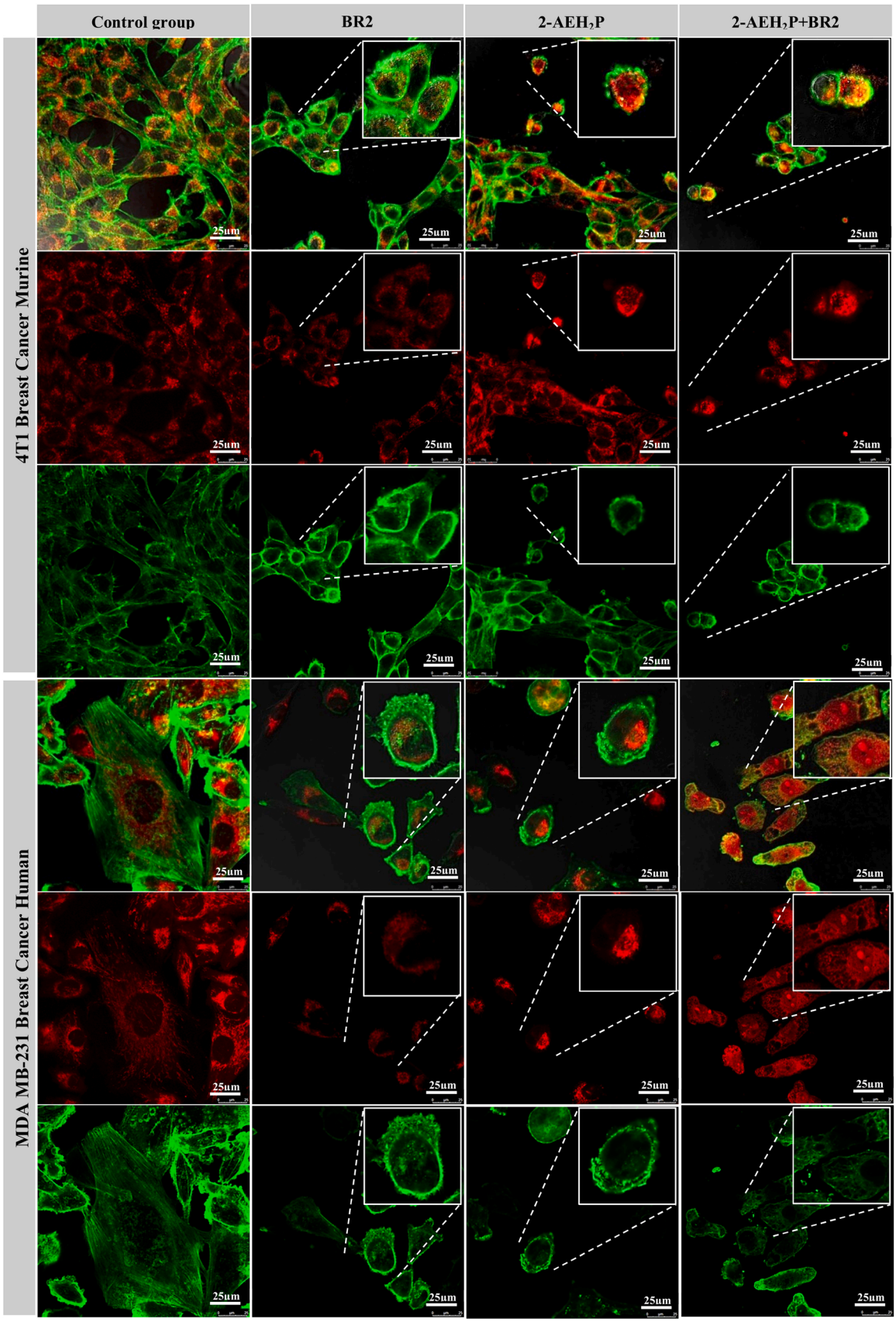

Fig. 5. Photomicrographs of MDA MB-231 and murine 4T1 triple-negative human breast cancer tumor cells with red-stained mitochondria (MitoRED) and green-stained cytoskeleton (phalloidin), analyzed by laser confocal microscopy. Tumor cells treated with the peptide BR2, the monophosphoester 2-AEH$_2$P, and the association 2-AEH$_2$P + BR2 at IC50 values for a period of 24 h.

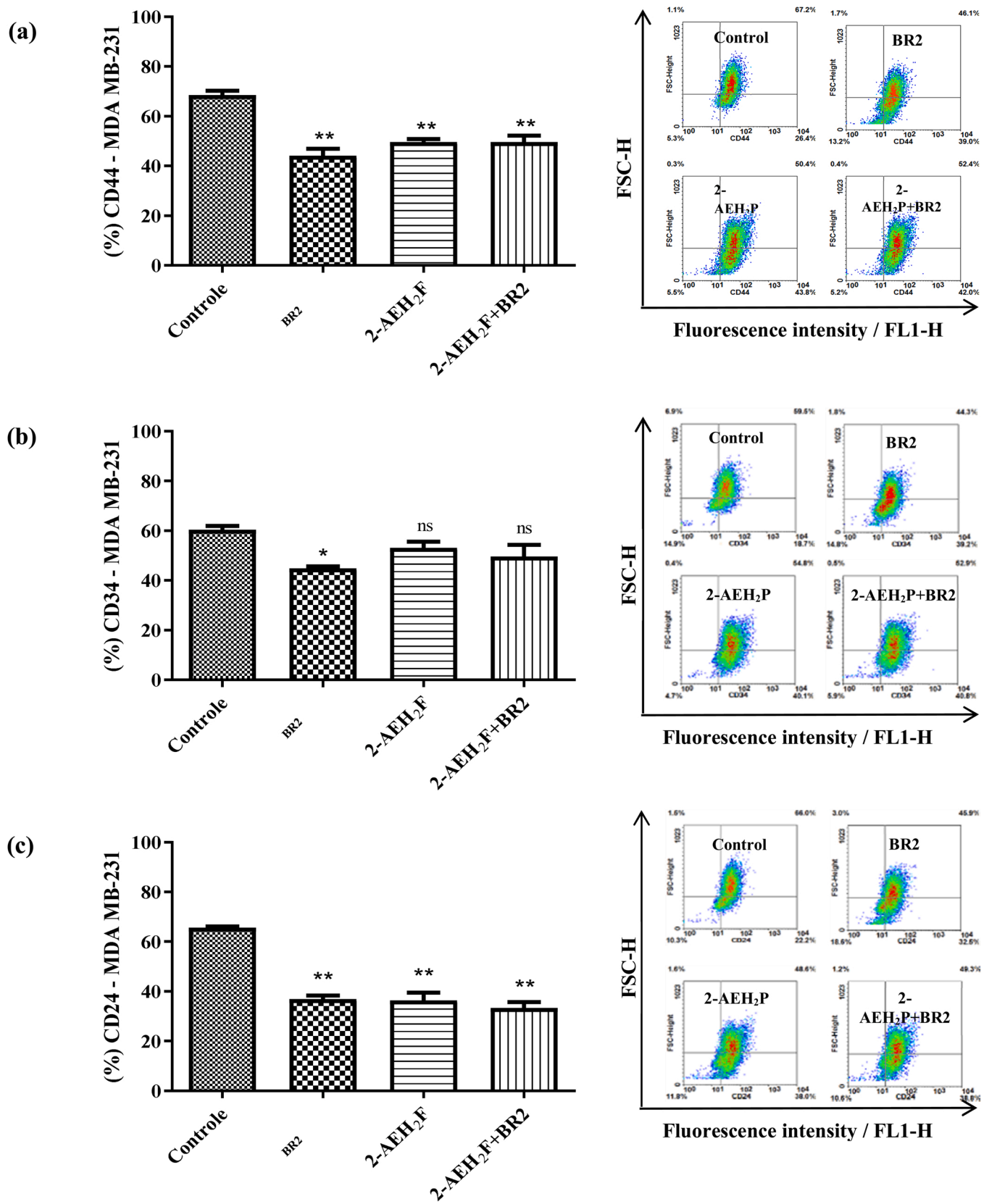

Fig. 6. Analysis of marker expression in MDA MB-231 human triple-negative breast cancer tumor cells. The expression of the markers was quantified by flow cytometry, after 24 h of treatment with the peptide BR2, the monophosphoester 2-AEH$_2$P and the association 2-AEH$_2$P + BR2 at IC50 values. (a) Expression of CD44; (b) Expression of CD34; (c) Expression of CD24. Bar graphs showing protein expression level as mean ± SD of three independent experiments. Representative Density Plots show the distribution of cell numbers with fluorescence intensity. Values are expressed as mean ± SD standard deviation of three independent experiments. Statistical differences were obtained by ANOVA and Tukey-Kramer multiple comparison tests. *$p < 0.05$, * *$p < 0.01$ and * **$p < 0.001$.

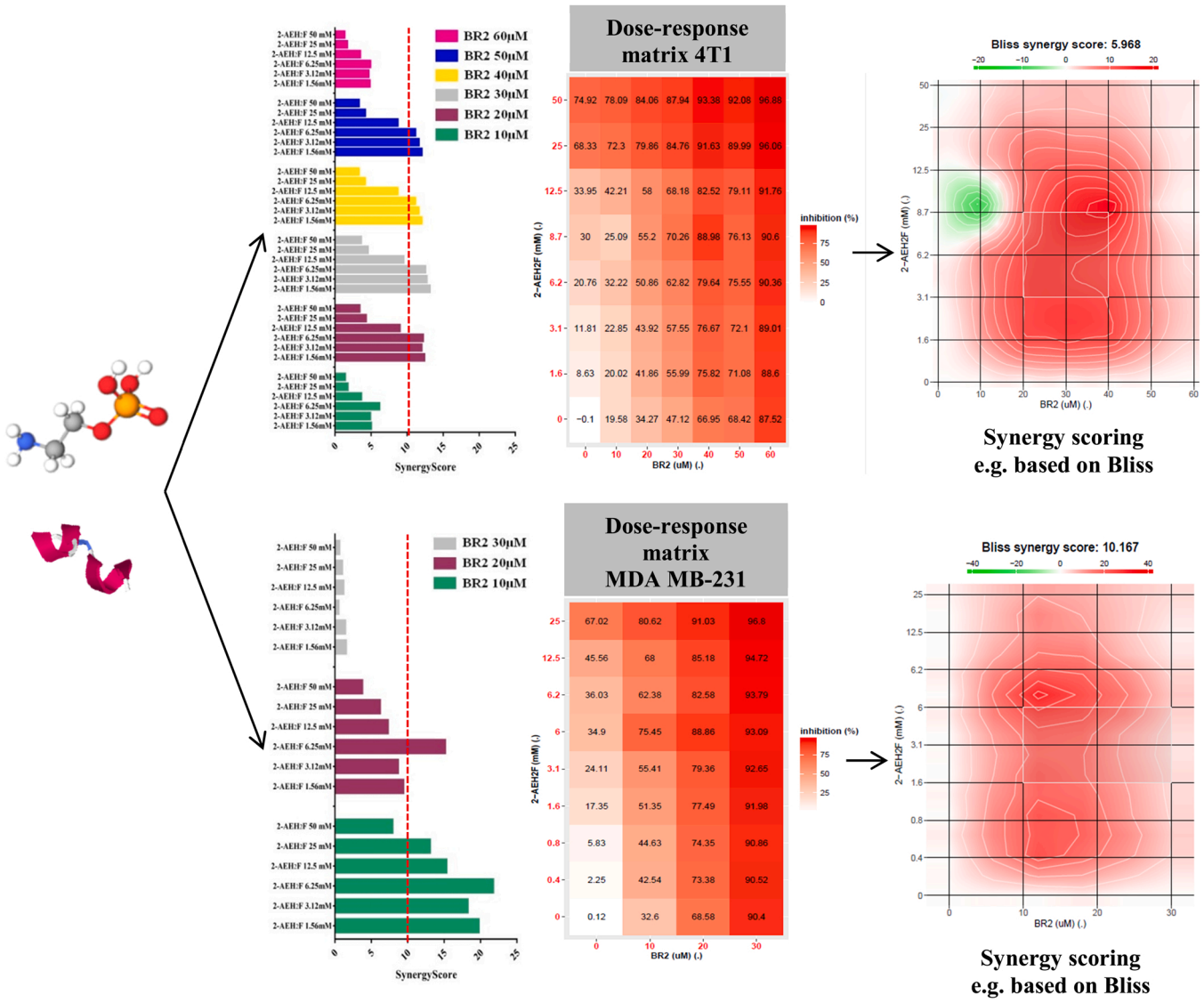

(a)

Cells	Drug combination	Synergy score	Effect	Method
4T1	BR2 (μM) - 2-AEH$_2$P (mM)	5.97	Additive	Bliss
MDA MB-231	BR2 (μM) - 2-AEH$_2$P (mM)	10.17	Synergistic	Bliss

Fig. 7. Determination of the additive and synergistic effect of the association of BR2 peptide with monophosphoester 2-AEH$_2$P on MDA MB-231 and murine 4T1 triple-negative breast cancer tumor cells. (a) Bar graphs show additive or synergistic additivity for concentrations of molecules in 4T1 and MDA MB-231 tumor cells. The antagonistic effect is observed in the colored space between white and green ($\leq$0), the additive effect and synergism are observed in the colored space between white and red ($>$ 0 and $<$10 additive; $>$ 10 synergistic). Color saturation is proportional to the magnitude of the difference between these values; (b) Table showing drug combination and synergy score for that combination.

lungs of immunodeficient mice [37]. CD24 expression has been associated with an adverse prognosis in ovarian cancer, non-small lung cancer cells, and prostate cancer [38]. Confirmation of this finding in breast cancer underscores the importance of CD24 in the disease progression of human carcinomas [38]. The present work evidences the reduction of these markers after the treatments, both when using the compounds separately and with the association, indicating the relevance of this strategy in the modulation of tumor aggressiveness, progression, and metastasis.

The increase of P53, P21, of cells in the G0/G1 phase and reduction of Cyclin D1 in 2-AEH$_2$P + BR2-treated cells may be an indication that the senescence pathway is being activated together with apoptosis. The ARF-P53 pathway is a crucial activator of this pathway, where the ARF protein stabilizes P53 levels by inactivating MDM2, enabling post-transcriptional activation of P21, inactivating CDKs, among them cyclin D1, causing proteins in the retinoblastoma to promote the cell cycle in G1 phase [39].

The mitochondrial cell death pathway is initiated by stress signals

through the release of apoptogenic factors such as cytochrome c, mediated by the reduction of the anti-apoptotic protein Bcl-2, promoting mitochondrial membrane permeabilization and cytochrome c release [40]. This release triggers caspase-3 activation through the formation of the apoptosome cytochrome c/Apaf-1/caspase-9 complex [41]. We can observe the reduction in the expression of important markers, directly related to cell death by intrinsic pathway, such as reduction of Bcl-2, increase of Bax and release of cytochrome c in the cytoplasm, which leads to believe that this pathway is active, and leads to the death of tumor cells.

Additional studies should be conducted to elucidate the mechanism of action directly involved in the apoptotic and antiproliferative effect of the BR2 peptide, the 2- AEH_2P, and their association. However, the data presented here demonstrate, effectively, the involvement of the death and senescence pathways, indicating that the association between the BR2 peptide and 2- AEH_2P has a greater antitumor potential than the isolated molecules.

5. Conclusions

The BR2 peptide at concentrations of IC50 of breast tumor cells showed no significant hemolytic effect. The association of 2-AEH_2P + BR2 promoted cytotoxicity in the studied tumor cell lines, in comparison with 2-AEH_2P. Furthermore, the BR2 peptide caused an arrest in the S phase for the MDA MB-231 tumor cells and G0/G1 for the 4T1 tumor cell, the association 2-AEH_2P + BR2 caused an arrest in the G0/G1 phases for the 4T1 Cells. and MDA MB-231 tumor cells. MDA MB-231 tumor cells were more sensitive to all treatments, promoting changes in cell morphology, especially in mitochondria, which lose their integrity and reorganize themselves in the perinuclear region, increasing the percentage of cells with inactive mitochondria. The BR2 peptide and the association 2-AEH_2P + BR2 were effective in inducing death in MDA MB-231 tumor cells, modulating the death and senescence pathways promoting: a decrease in cyclin D1 and Bcl-2 expression, p21 and Bax release of isolated cytochrome c on 2-AEH_2P. The values obtained with the proliferation rate showed a considerable decrease in the proliferative response of tumor cells after treatments, validating the reduction in the expression of the PCNA marker. The reduction of CD44, CD34, and CD24 markers related to the aggressiveness profile, progression, and tumor metastasis was evidenced. The result obtained in breast cancer cells demonstrates the pharmacological potential of treatments with cytotoxic effects and control of tumor progression, obtaining IC50 values two to three times lower in normal cells.

Declaration of Competing Interest

The authors declare that they have no known competing financial interests or personal relationships that could have appeared to influence the work reported in this paper.

Acknowledgments

Fapesp (State Research Support Foundation Sao Paulo - 2017/26355-0) Capes (Coordination for the Improvement of Higher Education Personnel - 88882.328116/2019-01) CNPq (National Council for Scientific and Technological Development - 305056/2019-0).

Appendix A. Supporting information

Supplementary data associated with this article can be found in the online version at doi:10.1016/j.biopha.2022.113398.

References

[1] F. Bray, J. Ferlay, I. Soerjomataram, R.L. Siegel, L.A. Torre, A. Jemal, Global cancer statistics 2018: GLOBOCAN estimates of incidence and mortality worldwide for 36 cancers in 185 countries, CA: A Cancer J. Clin. 68 (6) (2018) 394–424, https://doi.org/10.3322/caac.21492.

[2] J. Ferlay, M. Colombet, I. Soerjomataram, et al., Cancer statistics for the year 2020: An overview, Int. J. Cancer 149 (4) (2021) 778–789, https://doi.org/10.1002/ijc.33588.

[3] Brasil Ministério da Saúde; Estimativa 2020: Incidencia de câncer no Brasil. Instituto Nacional do Câncer José de Alencar Gomes da Silva. 2020;1:1–122.

[4] N.U. Lin, E. Claus, J. Sohl, A.R. Razzak, A. Arnaout, E.P. Winer, Sites of distant recurrence and clinical outcomes in patients with metastatic triple-negative breast cancer: High incidence of central nervous system metastases, Cancer 113 (10) (2008) 2638–2645, https://doi.org/10.1002/cncr.23930.

[5] R. Dent, M. Trudeau, K.I. Pritchard, et al., Triple-negative breast cancer: clinical features and patterns of recurrence, Clin. Cancer Res. 13 (15) (2007) 4429–4434, https://doi.org/10.1158/1078-0432.CCR-06-3045.

[6] L. Yin, J.J. Duan, X.W. Bian, S.C. Yu, Triple-negative breast cancer molecular subtyping and treatment progress, Breast Cancer Res. 22 (1) (2020), https://doi.org/10.1186/s13058-020-01296-5.

[7] R. van der Meel, E. Sulheim, Y. Shi, F. Kiessling, W.J.M. Mulder, T. Lammers, Smart cancer nanomedicine, Nat. Nanotechnol. 14 (11) (2019) 1007–1017, https://doi.org/10.1038/s41565-019-0567-y.

[8] J. Wolfram, M. Ferrari, Clinical cancer nanomedicine, Nano Today 25 (2019) 85–98, https://doi.org/10.1016/j.nantod.2019.02.005.

[9] R. Qiao, K. Wang, J. Zhong, Tumor-penetrating peptides. Peptide Applications in Biomedicine, Biotechnology and Bioengineering, Elsevier Inc, 2018, pp. 371–386, https://doi.org/10.1016/B978-0-08-100736-5.00014-4.

[10] S.A. Jang, H. Kim, J.Y. Lee, et al., Mechanism of action and specificity of antimicrobial peptides designed based on buforin IIb, Pept. (NY) 34 (2) (2012) 283–289, https://doi.org/10.1016/j.peptides.2012.01.015.

[11] Park C.B., Yi K.S., Matsuzaki K., Kim M.S., Kim S.C. Structure-Activity Analysis of Buforin II, a Histone H2A-Derived Antimicrobial Peptide: The Proline Hinge Is Responsible for the Cell-Penetrating Ability of Buforin II.; 2000. www.pnas.orgcgidoi10.1073pnas.150518097.

[12] E. Ruoslahti, Tumor penetrating peptides for improved drug delivery, Adv. Drug Deliv. Rev. 110–111 (2017) 3–12, https://doi.org/10.1016/j.addr.2016.03.008.

[13] J.H. Jang, Y.J. Kim, H. Kim, S.C. Kim, J.H. Cho, Buforin IIb induces endoplasmic reticulum stress-mediated apoptosis in HeLa cells, Pept. (NY) 69 (2015) 144–149, https://doi.org/10.1016/j.peptides.2015.04.024.

[14] Manuela Garcia Laveli da Silva, Luciana Bastianelli Knop, Durvanei Augusto Maria, Meclizine chloridrate and methyl-β-cyclodextrin associated with monophosphoester synthetic phosphoethanolamine modulating proliferative potential in triple-negative breast cancer cells, J. Pharm. Pharmacol. 7 (7) (2019), https://doi.org/10.17265/2328-2150/2019.07.006.

[15] A.K. Ferreira, R. Meneguelo, A. Pereira, O.M.R. Filho, G.O. Chierice, D.A. Maria, Synthetic phosphoethanolamine induces cell cycle arrest and apoptosis in human breast cancer MCF-7 cells through the mitochondrial pathway, Biomed. Pharmacother. 67 (6) (2013) 481–487, https://doi.org/10.1016/j.biopha.2013.01.012.

[16] T.O. Conceição, L.G.S. Cabral, M.G. Laveli-Silva, et al., New potential antiproliferative monophosphoester 2-aminoethyl dihydrogen phosphate in K-562 and K-562 MDR+ leukemia cells, Biomed. Pharmacother. (2021) 142, https://doi.org/10.1016/j.biopha.2021.112054.

[17] A.C. Luna, L. de, G.K.V. Saraiva, G.O. Chierice, H. Hesse, D.A. Maria, Antiproliferative and proapoptotic effects of DODAC/synthetic phosphoethanolamine on hepatocellular carcinoma cells, BMC Pharmacol. Toxicol. 19 (1) (2018), https://doi.org/10.1186/s40360-018-0225-2.

[18] A.C. de Lima Luna, G.K. Viegas Saraiva, O.M. Ribeiro Filho, et al., Potential antitumor activity of novel DODAC/PHO-S liposomes, Int. J. Nanomed. 11 (2016) 1577–1591, https://doi.org/10.2147/IJN.S90850.

[19] A.C.D.L. Luna, J.R.D.A. Santos Filho, H. Hesse, S.C. Neto, G.O. Chierice, D. A. Maria, Modulation of pro-apoptotic effects and mitochondrial potential on B16F10 cells by DODAC/PHO-S liposomes, BMC Res. Notes 11 (1) (2018), https://doi.org/10.1186/s13104-018-3170-7.

[20] M.D.T. Torres, C.N. Pedron, I. Araújo, P.I. Silva, F.D. Silva, V.X. Oliveira, Decoralin analogs with increased resistance to degradation and lower hemolytic activity, ChemistrySelect 2 (1) (2017) 18–23, https://doi.org/10.1002/slct.201601590.

[21] X. Liu, F. Wu, Y. Ji, L. Yin, Recent advances in anti-cancer protein/peptide delivery, Bioconjugate Chem. 30 (2) (2019) 305–324, https://doi.org/10.1021/acs.bioconjchem.8b00750.

[22] B.K. Gan, C.Y. Yong, K.L. Ho, A.R. Omar, N.B. Alitheen, W.S. Tan, Targeted delivery of cell penetrating peptide virus-like nanoparticles to skin cancer cells, Sci. Rep. 8 (1) (2018), https://doi.org/10.1038/s41598-018-26749-y.

[23] P.P. Czupiel, V. Delplace, M.S. Shoichet, Cationic block amphiphiles show anti-mitochondrial activity in multi-drug resistant breast cancer cells, J. Control. Release 305 (2019) 210–219, https://doi.org/10.1016/j.jconrel.2019.04.045.

[24] X. Zhang, C. Lin, A. Lu, et al., Liposomes equipped with cell penetrating peptide BR2 enhances chemotherapeutic effects of cantharidin against hepatocellular carcinoma, Drug Deliv. 24 (1) (2017) 986–998, https://doi.org/10.1080/10717544.2017.1340361.

[25] F. Shafiee, M. Rabbani, A. Jahanian-Najafabadi, Production and evaluation of cytotoxic effects of DT386-BR2 fusion protein as a novel anti-cancer agent, J. Microbiol. Methods 130 (2016) 100–105, https://doi.org/10.1016/j.mimet.2016.09.004.

[26] S. Marqus, E. Pirogova, T.J. Piva, Evaluation of the use of therapeutic peptides for cancer treatment, J. Biomed. Sci. 24 (1) (2017), https://doi.org/10.1186/s12929-017-0328-x.

[27] W. Huang, J. Seo, S.B. Willingham, et al., Learning from host-defense peptides: cationic, amphipathic peptoids with potent anticancer activity, PLoS ONE 9 (2) (2014), https://doi.org/10.1371/journal.pone.0090397.
[28] A.K. Ferreira, R. Meneguelo, A. Pereira, O.M.R. Filho, G.O. Chierice, D.A. Maria, Anticancer effects of synthetic phosphoethanolamine onEhrlich ascites tumor: an experimental study, Anticancer Res. 32 (2012) 95–104.
[29] B. Nami, H. Maadi, Z. Wang, Mechanisms underlying the action and synergism of trastuzumab and pertuzumab in targeting HER2-positive breast cancer, Cancers (Basel) 10 (10) (2018), https://doi.org/10.3390/cancers10100342.
[30] S. Sreenivasan, S. Krishnakumar, Synergistic effect of curcumin in combination with anticancer agents in human retinoblastoma cancer cell lines, Curr. Eye Res. 40 (11) (2015) 1153–1165, https://doi.org/10.3109/02713683.2014.987870.
[31] M.S. Jabir, A.A. Taha, U.I. Sahib, Z.J. Taqi, A.M. Al-Shammari, A.S. Salman, Novel of nano delivery system for Linalool loaded on gold nanoparticles conjugated with CALNN peptide for application in drug uptake and induction of cell death on breast cancer cell line, Mater. Sci. Eng. C. 94 (2019) 949–964, https://doi.org/10.1016/j.msec.2018.10.014.
[32] L. Ayalew, J. Acuna, S.F. Urfano, et al., Conjugation of paclitaxel to hybrid peptide carrier and biological evaluation in jurkat and A549 cancer cell lines, ACS Med. Chem. Lett. 8 (8) (2017) 814–819, https://doi.org/10.1021/acsmedchemlett.7b00117.
[33] S. Valastyan, R.A. Weinberg, Tumor metastasis: molecular insights and evolving paradigms, Cell 147 (2) (2011) 275–292, https://doi.org/10.1016/j.cell.2011.09.024.
[34] C. Sheridan, H. Kishimoto, R.K. Fuchs, et al., CD44+/CD24-breast cancer cells exhibit enhanced invase properties: an early step necessary for metastasis, Breast Cancer Res. 8 (5) (2006), https://doi.org/10.1186/bcr1610.
[35] Lopez J.I., Camenisch T.D., Stevens M.V., Sands B.J., Mcdonald J., Schroeder J.A. CD44 Attenuates Metastatic Invasion during Breast Cancer Progression.; 2005. http://aacrjournals.org/cancerres/article-pdf/65/15/6755/2533483/6755–6763.pdf.
[36] A. Hill, S. McFarlane, K. Mulligan, et al., Cortactin underpins CD44-promoted invasion and adhesion of breast cancer cells to bone marrow endothelial cells, Oncogene 25 (45) (2006) 6079–6091, https://doi.org/10.1038/sj.onc.1209628.
[37] Z.F. Yang, D.W. Ho, M.N. Ng, et al., Significance of CD90+ cancer stem cells in human liver cancer, Cancer Cell 13 (2) (2008) 153–166, https://doi.org/10.1016/j.ccr.2008.01.013.
[38] Kristiansen G., Rgen Winzer K.J., Mayordomo E., et al. *CD24 Expression Is a New Prognostic Marker in Breast Cancer*.; 2003. ⟨http://aacrjournals.org/clincancerres/article-pdf/9/13/4906/2087194/df1303004906.pdf⟩.
[39] D. Muñoz-Espín, M. Serrano, Cellular senescence: from physiology to pathology, Nat. Rev. Mol. Cell Biol. 15 (7) (2014) 482–496, https://doi.org/10.1038/nrm3823.
[40] S. Fulda, K.M. Debatin, Extrinsic versus intrinsic apoptosis pathways in anticancer chemotherapy, Oncogene 25 (34) (2006) 4798–4811, https://doi.org/10.1038/sj.onc.1209608.
[41] X. Saelens, N. Festjens, L. vande Walle, M. van Gurp, G. van Loo, P. Vandenabeele, Toxic proteins released from mitochondria in cell death, Oncogene 23 (16 REV. ISS. 2) (2004) 2861–2874, https://doi.org/10.1038/sj.onc.1207523.